Prenatal stress induces transient developmental alterations in distinct GABAergic populations and leads to long-lasting behavioral abnormalities

Keren Shoshani-Haye [a,b], Gilgi Friedlander [c], Ofra Golani [d], Suellen Almeida-Correa [a,b], Yair Shemesh [a,b], Alon Chen [a,b,*]

[a] Department of Molecular Neuroscience, Weizmann Institute of Science, Rehovot, Israel
[b] Department of Brain Sciences, Weizmann Institute of Science, Rehovot, Israel
[c] The Crown Genomics Institute of the Nancy and Stephen Grand Israel National Center for Personalized Medicine, Weizmann Institute of Science, Rehovot, Israel
[d] MICC Cell Observatory, Department of Life Sciences Core Facilities, Weizmann Institute of Science, Rehovot, Israel

ARTICLE INFO

ABSTRACT

Prenatal stress (PNS) is a well-established risk factor for psychiatric disorders, yet the underlying neurobiological mechanisms remain unclear. Here, we demonstrate that PNS induces long-term behavioral abnormalities, including increased anxiety- and depressive-like behaviors specifically in adult male mice. To investigate potential neurodevelopmental disruptions, we analyzed the medial prefrontal cortex (mPFC) at key postnatal stages. RNA sequencing at postnatal day 1 (P1) revealed significant transcriptional changes, particularly in genes associated with neuronal migration and differentiation, with a diminished effect by P14. Histological analysis identified a transient imbalance in inhibitory neuron subpopulations, PNS decreased the density of early-born neurons derived from the medial ganglionic eminence (MGE) while increasing late-born neurons derived from the caudal ganglionic eminence (CGE) at P1. EdU labeling confirmed that these shifts were time- and subtype-specific, affecting inhibitory neuron proliferation at distinct embryonic stages. By P15, these neuroanatomical alterations largely resolved, yet behavioral abnormalities persisted into adulthood. Our findings suggest that PNS disrupts inhibitory neuron development during a critical early window, leading to lasting behavioral consequences despite the transient nature of anatomical changes. This study highlights the selective vulnerability of inhibitory neuron subtypes to early-life stress and provides insight into potential mechanisms underlying stress-related psychiatric disorders.

1. Introduction

Early in development, the brain undergoes extensive dynamic changes and is highly susceptible to changes in the *in-utero* environment. Alterations in maternal nutrients and hormones, might have a profound effect on cortical development and can result in lasting, and in some cases also latent, behavioral programming of the embryo (Almond and Currie, 2011; Vasistha and Khodosevich, 2021). Exposure to PNS, in particular, was shown to lead to long-lasting behavioral and physiological implications. Children born right after the Dutch Hunger Winter or the Chinese famine, for example, were found to be at an increased risk to develop psychiatric disorders, including major depression disorder (MDD) and schizophrenia (Brown et al., 1995; Franzek et al., 2008; Hoek et al., 1998; St Clair, 2005). Other longitudinal studies further associate prenatal maternal exposure to stress with offspring depression

and anxiety later in life (Fraser et al., 2012; Kolominsky et al., 1999). These effects are thought to be mediated, at least in part, by elevated maternal cortisol levels and the subsequent increase in cortisol levels reaching the developing embryo (Buss et al., 2012; Seckl and Meaney, 2004).

The effect of prenatal maternal stress can be modeled in animals. Animal models of PNS ranged from tail suspension, crowding, repeated shocks, restraint, and immobilization to stressors such as white noise and flashing lights. These stressors are repeated several times per day in some protocols, while others use varying stressors, subjecting the animals to unpredictable stressors daily (Boersma and Tamashiro, 2015; Weinstock, 2017). Mice exposed to PNS are characterized by alterations in a wide range of behaviors including cognitive, metabolic and social behaviors (Weinstock, 2008). Here we focus on affective outcomes, as these represent the most consistently reported and clinically relevant

phenotype associated with PNS. Using these models, it was shown that mice exposed to PNS are characterized by an increase in anxiety-like and depressive-like phenotypes as measured by the open field test, elevated plus maze, tail suspension and forced swim test (Enayati et al., 2020; Estanislau and Morato, 2005; Jafari et al., 2017; Morley-Fletcher et al., 2004; Mueller and Bale, 2008). These results vary depending on the severity, duration and gestational period of the stressors; however, they consistently indicate an increase in anxiety- and depressive-like behaviors in response to different stress paradigms.

The specific mechanism through which maternal stress increases disease risk remains unclear; however, several key contributors have been proposed, particularly involving cortical inhibitory neurons and their development. Most cortical inhibitory neurons are derived from two main populations, born in the medial and caudal ganglionic eminence (Kelsom and Lu, 2013; Miyoshi et al., 2010; Miyoshi and Fishell, 2011). MGE-derived inhibitory neurons account for around 60 % of inhibitory neurons and give rise mainly to parvalbumin (PV)-expressing and somatostatin (SST)-expressing subtypes, which predominantly target pyramidal neurons. The CGE-derived neurons comprise around 30 % of inhibitory cortical neurons and often modulate the activity of other inhibitory neurons. Half of these co-express RELN and the other fractions expresses vasoactive intestinal peptide (VIP) (Laclef and Métin, 2018; Lim et al., 2018; Llorca and Deogracias, 2022; Miyoshi et al., 2010; Miyoshi and Fishell, 2011). Inhibitory neuronal subtypes differ in time of birth and migration. MGE interneurons are born as early as embryonic day (E)9.5, with SST cell birth peaking at E11.5 and PV at E14.5. The CGE is responsible for producing late born interneurons peaking at E16.5. Both MGE- and CGE-derived inhibitory neurons migrate tangentially to reach the cortical plate, where they then migrate radially to reach the proper cortical layer. Most of migration is completed by birth. As neurons reach their proper cortical location, they grow axons and dendrites and form neuronal circuits.

Proper timing and placement of inhibitory neurons during development are essential to proper synaptic connectivity and network formation (Bollmann et al., 2023; Duan et al., 2020; Modol et al., 2020). Delayed migration and cortical layering can disrupt network connectivity, a common pathophysiology of neurodevelopmental and psychiatric disorders associated with PNS, such as Schizophrenia and MDD (Markham and Koenig, 2010). Previous studies have shown that changes in the *in-utero* environment can lead to impairment in inhibitory neuron development (reviewed by Vasistha and Khodosevich, 2021). For example, fetal cocaine exposure results in impairment of interneuron migration (McCarthy et al., 2011). Additionally, maternal inflammation was shown to cause a reduction in GAD67+ cortical migration with a specific decrease in PV+ and SST + neurons detected also two weeks postnatally (Vasistha et al., 2019). Improper cortical development was also shown in the context of prenatal psychogenic stress. Prenatal restraint stress resulted in a reduction in GABAergic neurons progenitors in the telencephalon during embryogenesis, accompanied by a reduction of dlx2 and nkx2.1 transcription factors, which regulate interneuron migration (Lussier and Stevens, 2016; Stevens et al., 2013). Thus, inhibitory neurons display a vulnerability to stress and other insults, with different subtypes being differentially affected. However, while maternal psychogenic stress has also been linked to improper cortical development, its specific effects on inhibitory neuron subtypes remain unexplored.

Here, we use chronic variable stress in pregnant dams to induce PNS on offspring and show long lasting behavioral abnormalities in the adult offspring, including increased anxiety- and depressive-like behaviors. RNA sequencing of the mPFC at P1 revealed transcriptional alterations in genes related to neuronal migration and differentiation particularly of inhibitory neurons. These alterations largely diminished by P14. Anatomical analysis at P1 showed a transient but significant shift in the balance of inhibitory neuron subtypes with an increased density of CGE-derived interneurons and a decreased density of MGE-derived populations. EdU labeling further demonstrated that PNS alters the timing of interneuron proliferation in a subtype-specific manner. Although these anatomical changes were largely resolved by P15, the early disruption of inhibitory neuron development and cortical layering likely contributes to lasting synaptic and circuit level alterations, leading to behavioral dysfunction. Together, our findings reveal a transient, developmentally timed impairment in inhibitory circuit formation within the mPFC and highlight the selective vulnerability of interneuron subtypes to PNS.

2. Materials and methods

2.1. Mice handling

ICR mice (Harlan Sprague Dawley Inc., Indianapolis, IN) were maintained in a temperature-controlled (22 ± 1 C) mouse facility on a reverse 12 h light-dark cycle at the Weizmann Institute of Science, according to institutional guidelines. Food and water were given *ad libitum*. All experimental protocols were approved by the Institutional Animal Care and Use Committee (IACUC) of The Weizmann Institute of Science.

Mating: ICR female mice at the age of 11–13 weeks were mated with ICR proven breeders and checked twice a day for a copulation plug. Once a plug was detected (denoted GD0.5), females were randomly assigned to stress or control group.

Weaning: Mice used for behavioral tests were weaned at the age of P25 and cohoused with littermates according to sex in dark light cycle (10:00–22:00).

2.2. PNS protocol

PNS protocol was conducted as previously reported (Schroeder et al., 2018a, 2018b). In short, from GD1.5 to GD16.5, pregnant dams were exposed to a chronic mild stress protocol that includes two short manipulations per day during the dark phase and a further manipulation during the light phase of the day. The short stressors include cage tilt, no bedding, water in cage, white noise, elevated platform, restraint and swim stress. The light-phase manipulations include illumination, saturated bedding, novel object and overcrowding.

2.3. Maternal postnatal behavior

As previously described (Schroeder et al., 2018a, 2018b), pregnant dams were transferred on GD17 to cages containing a black acrylic shelter that is seen through under infrared light and infrared camera, and left undisturbed. Following birth, dams were recorded twice a week during the dark phase for 2.5 h at a time. For frequency analysis-each mother was observed every 5 min for 5 s. A total of 28 time points (from min 15 to min 150, 5 min intervals) were evaluated. A single behavior from the following list was assigned for each time points: nursing, non-nutritive contact, self-grooming, eating, drinking, resting, activity (mother exploring the cage and not in the nest). For entropy rate analysis-mothers were observed continuously for 180 min and behaviors were recorded as discrete sequences of the behaviors mentioned above. Entropy rate was calculate as previously reported (Davis et al., 2017). In short, we created a matrix of transition probabilities between all pairs of discrete maternal behaviors by normalizing the number of transitions from each behavior. We then calculated the stationary distribution of the resulting first-order, time-homogeneous Markov chain and used it to compute the Shannon entropy rate as a measure of behavioral predictability.

2.4. Behavioral tests

Before each behavioral test, mice were moved to the test room and habituated for at least 1-h prior testing. All tests took place in the middle of the dark phase. Mice were single housed throughout behavioral

testing.

2.4.1. Open-field test

Open field test was performed in a 50 X 50 X 22-cm grey box, lit to 120 lux. The mice were placed in the corner of the box and tracked for 10 min. Locomotion in the box was quantified using a video tracking system (EthoVision). As proximity to the walls is an anxiety-related behavior (Seibenhener and Wooten, 2015), a smaller 25 × 25 cm zone in the center of the arena was programmed into the software tracking system. Total distance moved, time spent in the center zone, and time inactive were calculated using the tracking system.

2.4.2. Forced swim test

Mice were placed for 6 min inside plastic cylinders (height 25 cm, diameter 18 cm), containing 12 cm of water maintained at 25 ± 1 °C. The session was videotaped for later analysis. Analysis of videotape was performed using video tracking system (EthoVision). The duration of immobility was monitored during the last 4 min of the 6-min test. Immobility period was defined as the time spent by the animal floating in the water without struggling, making only those movements necessary to keep its head above the water.

2.4.3. Home-cage locomotion

Was assessed using the InfraMot system (TSE Systems). Mice were housed individually for 90h, in which the first 18h were considered habituation to the individual housing conditions (16:00–10:00). Measurements of general locomotion consisted of three light and three dark cycles in the last 72 h collected at 30 min intervals (dark begins at 10am).

2.5. Tissue extraction and cryodissections

Brains were extracted within 3 min from time of decapitation and snap frozen in 2-methylbutane on dry ice and stored at −80 °C. Brains were embedded in O.C.T and 200 μm thick coronal sections were sliced on a cryostat. mPFC were collected using biopsy punch tools with inner diameter of 0.8 mm for brains collected at P1 (FST, Item No. 18035-80), and 1.2 mm for brains collected at P14 (EMS, Cat#. 69039-12). mPFC region was detected and extracted based on atlas for the developing mouse brain (Paxinos et al., 2020).

2.6. RNA sequencing and analysis

2.6.1. RNA library preparation

RNA was extracted using RNAeasy micro kit (Qiagen) according to manufacturer's protocol. Sequencing Libraries were prepared using an in-house poly-A based RNA-seq protocol. Briefly, total RNA was fragmented followed by reverse transcription and second strand cDNA synthesis. The double-strand cDNA was subjected to end repair, A base addition, adapter ligation and PCR amplification to create libraries. Libraries were evaluated by Qubit and TapeStation. All libraries had an RIN above 8.0.

2.6.2. RNA sequencing data preprocessing and QC

Sequencing libraries were constructed with barcodes to allow multiplexing of samples on a single lane of Illumina NovaSeq S1 (200 cycles), resulting in a median of 59.5M paired end 100X2-bp reads per sample. 93.4 % of reads had a Phred score greater than 30, with a total average of Q = 34.41. Poly-A/T stretches and Illumina adapters were trimmed from the reads using Cutadapt (version 2.7) (parameters: -times 2 -O 5 -m 25 -q 10 -e 0.1) (Martin, 2011). Reads shorter than 25bp after trimming were discarded (1.0 % of reads). Reads were mapped to the M. musculus reference genome GRCm38 using STAR (version 2.7.3a) (Dobin et al., 2013), supplied with gene annotations downloaded from Ensembl (and with EndToEnd option and outFilterMismatchNoverLmax was set to 0.04). Mapping of reads to the genome resulted in 90.0 % of

reads being mapped. Furthermore, 90.1 % of the uniquely mapped reads were found counted on exons, resulting in a final median of 45.9M reads per sample. Expression levels for each gene were quantified using htseq-count (Anders et al., 2015), using the gtf above. RNA sequencing data generated in this study have been deposited in the NCBI Gene Expression Omnibus (GEO) (Edgar et al., 2002) under accession number GSE296365.

2.6.3. Differential expression analysis

Differentially expressed (DE) genes were identified using DESeq2 (version 1.26) (Love et al., 2014) with the betaPrior, cooksCutoff and independent filtering parameters set to False. Raw P values were adjusted for multiple testing using the procedure of Benjamini and Hochberg. Pipeline was run using snakemake (Mölder et al., 2021). Genes with adjusted p-values ≤ 0.05 and |fold change| ≥ 1.4 were considered DE.

2.6.4. Gene ontology

GO enrichment analysis was done using PANTHER with the over-representation test (Ashburner et al., 2000; Carbon et al., 2021). DE genes were used as an input and the background reference set was defined as all genes with a Max_count$\geq$5 in our data set (19,748 genes). Fisher test with FDR correction was conducted to detect enrichment in GO biological processes annotations. Significant Go terms (FDR ≤ 0.05) with at least 2 related DE genes are presented. Terms with more than 4000 genes were excluded as having wide meaning. Terms were grouped into eight clusters by hierarchical clustering of a binary term–gene matrix using Jaccard distance, as implemented in the ComplexHeatmap R package (Gu, 2022; Gu et al., 2016).

2.7. EdU injections

EdU (5-Ethynyl-2′-deoxyuridine, Lumiprobe, Geter) was dissolves in PBS for final concentration of 30 mM (7.6 mg/mL). Dams are injected Intraperitoneal with 0.05 mg/g at a single time-point.

### 2.8. Immunohistochemistry and imaging

2.8.1. Immunostaining

A description of antibodies used in this study is given in Supplementary Table 1. For immunofluorensense of P1 mice, mice were perfused with PBS, brains were submerged in 4 % paraformaldehyde (PFA) in PBS overnight and transferred to 4 % PFA with 30 % sucrose until further use. For cryosectioning samples were embedded in OCT and sectioned by cryostat at a thickness of 20 μm. Slices were mounted and all further steps were conducted on mounted slides. All steps were done at room temp unless mentioned otherwise. Slides were dried for 15min then treated with 10 mM Sodium citrate pH6 for 15min at 85 °C for antigen retrieval. After washing the tissue 3X5′ in TBS 0.5 % Triton, EdU click assay was done by treating the tissue for 30min with Cy5-azide (Karefast, FLP 025) 2.5 μM in a solution containing 100 mM Tris, 1 mM CuSO4, and 100 mM ascorbic acid in PBS. Samples were rinsed again in 3X5' in TBS 0.5 % Triton. For OPAL staining-slides were blocked with 0.6 % H2O2 diluted in TBS 0.5 % Triton for 1h, washed in PBS and blocked for 2h with 20 % NHS in 0.2 % Triton X-100 containing PBS. The following steps were repeated twice for each of the antibodies: primary antibody incubation with 2 % NHS and 0.5 % Triton X-100 O.N at 4 °C, PBS washes, Secondary HRP antibody incubation with 2 % NHS and 0.5 % Triton X-100 for 1.5h, PBS washes, Signal amplification using OPAL reagent for 15min in TSA buffer (prepared from 0.31gr boric acid and 5ul 30 % H2O2 in 50 ml DDW, adjusted pH8.5), PBS washed and antibody stripping in sodium citrate for 10min at 95 °C. after repeating these steps twice, nuclei were counterstained with DAPI for 3 min (1:500, Sigma), washed in PBS and coverslips were mounted on slides with aqua-poly/mount (Polysciences). To ensure no unspecific binding, a negative sample was run in each batch, treated with all same

conditions while leaving out mouse anti-Lhx6 primary antibody in the second iteration.

For immunofluorescence of P15 mice, mice were perfused with 4 % PFA in PBS, submerged in 4 % PFA O.N and transferred to 4 % PFA with 30 % sucrose until further use. For cryosectioning samples were embedded in OCT and sliced in a microtome at a thickness of 40 μm. Histology was conducted on floating sections. EdU Click-assay was conducted with similar concentrations as mentioned for P1 sample, with Cy3-azide (Karefast, FCC 147). For staining-sections were permeabilized for 1h in 0.2 % Triton X-100, blocked for 2h with 20 % NHS in 0.2 % Triton X-100 containing PBS. Subsequently, they were incubated for 48h at 4 °C with appropriate primary antibodies. The following day, sections were washed and then incubated with biotin overnight at 4 °C. Samples were washed again and incubated with Alexa Fluor conjugated Avidin and secondary antibodies for 2h at room temperature. Nuclei were counterstained with DAPI (1:1000, Sigma) and coverslips were mounted on slides with aqua-poly/mount (Polysciences).

2.8.2. Image acquisition and analysis

Images were acquired using Dragonfly confocal microscope system (Dragonfly 600 spinning disk, Andor Technology) with 20× oil objective. A 12um Z-stack montage is acquired in all relevant channels. Fiji was used for maximum intensity projection (Schindelin et al., 2012). Images were analyzed in QuPath (Bankhead et al., 2017) with extensions as followed. Cell segmentation was done using StarDist extension (Weigert and Schmidt, 2022) based on Dapi channel, using a model trained on representative images with the parameter CellExpansion set to 5 μm, and excluding nuclei with area that is larger than 350 μm^2 or smaller than 10 μm^2. Positive cell classification was done using QuPath built-in object classifier with random trees, using all shapes and all intensity parameters of the relevant channels. The classifiers were trained on representative region images from all conditions and automatically applied to all images. Regions of interest were annotated by aligning sections to the atlas of developing mouse brain (Paxinos et al., 2020) using Warpy extension (Chiaruttini et al., 2022). Values obtained from
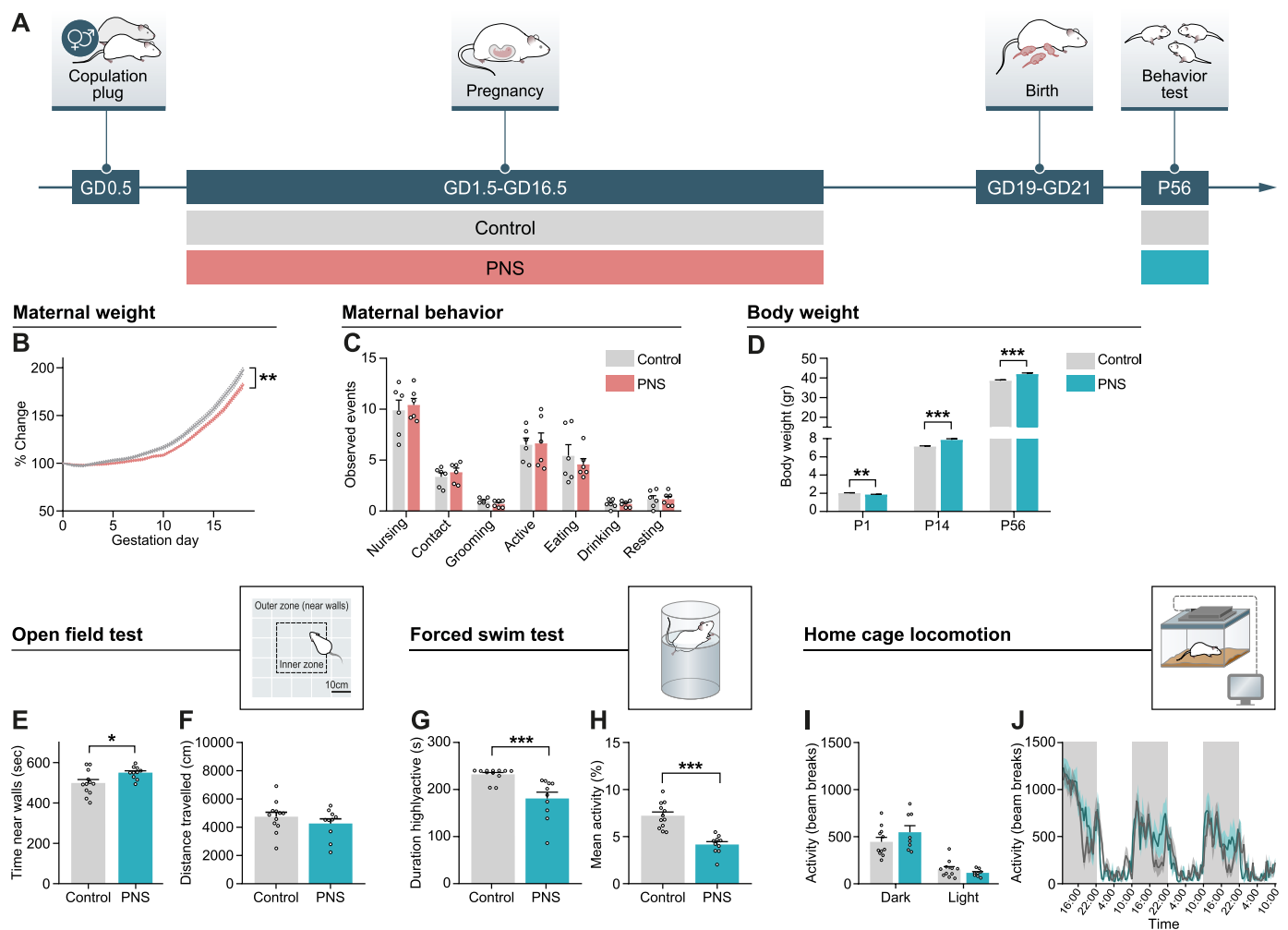
Fig. 1. Mice exposed to PNS Display an increase in anxiety- and depressive-like phenotype. (A) Prenatal stress protocol. During gestation, from GD1.5 to GD 16.5 dams are exposed to two short manipulations during the dark phase, and a further long manipulation during the entire light phase. The short manipulations include: cage changes, cage tilt, white noise, water in cage, no bedding, immobilization in a tube, elevated platform, swim in warm water. A further long manipulation during the light phase include: Illumination, saturated bedding (with water), novel object (marbles), and overcrowding. (B) Change in maternal weight during pregnancy. PNS dams show less increase in weight during gestation compared to control (repeated measure ANOVA F(1,53) = 9.892, p = 0.002). (C) Maternal behavior in the initial three weeks after birth. Each dam is monitored twice a week. The plot depicts the average number of events observed within the 6 sessions per mouse (n = 6 per group). (D) Weight of male littermates at P1 (t(35) = 2.88 q = 0.007), P14 (t(168) = 5.165 q < 0.0001), P56 (t(89) = 4.450 q < 0.0001). Benjamini, Krieger and Yekutieli correction for multiple comparisons. (E) Time spent near walls in the OF test (t(20) = 2.414 p = 0.025). (F) Distance traveled within the OF arena (t(20) = 1.039 p = 0.311). (G) Time spent highly active during the FST session (t(20) = 3.903, p = 0.0009). (H) Average activity during FST (t(20) = 5.906 p < 0.0001). (I) Locomotor activity averaged during dark and light hours (repeated measure ANOVA F(1,17) = 0.417 p = 0.527). (J) Home cage locomotor activity across time in HCL test. Bargraphs represent means, whiskers represent SEM.

three coronal sections of the mPFC were averaged to yield a single parameter for each subject.

2.9. Statistical analysis

Statistical analyses were performed using GraphPad Prism 8 (GraphPad software, Inc., La Jolla, CA). Tests included repeated measures ANOVA, t tests or one-way ANOVA when relevant. Differences between the groups were assessed using Sidak's multiple comparisons post-hoc. Specific details of N and tests used are provided in the figure legends.

3. Results

3.1. Mice exposed to PNS display an increase in anxiety- and depressive-like phenotype

In order to study the behavioral outcomes of PNS, we employ a model of chronic variable stress during gestation (Schroeder et al., 2018b). From gestation day 1.5 (GD1.5) to GD16.5, pregnant dams were exposed to PNS protocol that included two short manipulations per day during the dark phase and a further manipulation during the light phase of the day (Fig. 1A). As previously reported (Schroeder et al., 2018a, 2018b), PNS dams gained significantly less weight during gestation (Fig. 1B). In accordance with previous work, no differences were observed in pregnancy rate, GD at birth, survival of pups to weaning or litter size (Supplementary Fig. 1). To ensure the observed effects are a result of maternal stress during pregnancy rather than changes in postnatal maternal behavior, we monitored maternal behavior during the initial three weeks post birth. Mothers did not display changes in the frequency of pup- or self-oriented behaviors (Fig. 1C). As prenatal stress might affect the duration of each behavior bouts and the predictability of their sequence (Birnie and Baram, 2022, 2025) we additionally monitored for the number and duration of behavioral bouts, as well as frequency of behavioral transitions. Using these parameters, we calculated the entropy rate, a measure of behavioral predictability, and found no significant differences between groups (Supplementary Fig. 2). These results suggest that long lasting effects are more likely derived from the prenatal environment.

We examined the effect of PNS on both male and female offspring. PNS males were born with lower body weight, nevertheless, from P14 onward had higher body weight than control (Fig. 1D). We additionally tested for anxiety- and depressive-like behaviors in the open field test (OF) and the forced swim test (FST). In the open field test, PNS males spent more time near the walls, indicative of high anxiety-like behavior (Fig. 1E). No significant difference was observed in the total distance traveled in this test (Fig. 1F). Furthermore, males exposed to PNS showed a decrease in total activity time in the forced swim test (Fig. 1G), and in their mean activity level (Fig. 1H), indicative of a more depressive-like phenotype. Locomotor activity during light and dark phase was tracked in the home cage locomotion (HCL) system. No effect in locomotor activity was observed between PNS and control males in the HCL test (Fig. 1I and J). In comparison, female offspring showed a similar increase in body weight in adulthood and an increase in locomotor activity during the dark phase (Supplementary Fig. 3A–C), however, no significant differences were observed in measures of anxiety or depressive-like behavior (Supplementary Fig. 3D–G). PNS is known to affect offspring in a sexually dimorphic manner, with several studies reporting specifically males being more prone to develop anxiety- and depressive-like behaviors (Mueller and Bale, 2008; Van den Hove et al., 2013; Zuena et al., 2008). Given that our findings align with these observations, we have chosen to focus in this study on male offspring.

3.2. PNS alters transcription of genes associated with cellular migration

Clear alterations in male offspring behavior following exposure to

PNS were observed in our model and in several previously published studies in rodents and humans. Here, we were interested in examining whether these effects are mediated by differential gene expression at perinatal stages. Pregnant dams were randomly assigned to PNS and control groups, and brains of the offspring were collected at either one day postnatally (P1) or at two weeks of age (P14). RNA was extracted from the mPFC and differential comparison analysis of PNS vs. control was conducted per time-point. Genes with adjusted p-values ≤ 0.05 and |fold change| ≥ 1.4 were considered differentially expressed (DE).

PNS altered the expression of 74 genes at P1, whereas fewer DE genes were observed at P14 (Fig. 2A and B). Gene ontology enrichment analysis of DE genes at P1 revealed 53 enriched biological processes, with 48 out of the 74 DE genes linked to these terms. Clustering based on DE gene similarity resulted in 8 clusters, each representing different biological processes including extracellular organization, regulation of cell locomotion and embryonic development (Fig. 2C). No pathways were enriched in the DE gene set at P14. Of particular interest was cluster 4, which encompassed GO terms related to the regulation of cell locomotion, a process critical for neuronal migration during cortical development. A network graph of the GO terms in cluster 4 illustrates the relationships between DE genes and their associated biological processes (Fig. 2D). Among the 31 DE genes linked to these terms, many were related specifically to cellular locomotion in the cortex, and specifically at perinatal stages, such as igf2, serpinf1, enpp2, reln and nr2f2 (Bai et al., 2022; Greenman et al., 2015; Kelsom and Lu, 2013; Pardo et al., 2019; Vasistha and Khodosevich, 2021). Many of these genes serve specifically in the development of inhibitory neurons (Kelsom and Lu, 2013; Vasistha and Khodosevich, 2021).

3.3. PNS impairs the density of cells born at various embryonic days in the developing prefrontal cortex

Given the association of DE genes with cellular locomotion, we focused on anatomical assessment of cell birth and migration. We utilized 5-Ethynyl-2′-deoxyuridine (EdU) labeling to mark cells born at the time of injection and track their subsequent localization within the cortex. Pregnant dams in the PNS and control groups were injected with EdU at one of three timepoints corresponding to embryonic days E11.5, E14.5 or E16.5 (Fig. 3A). Similar to RNA seq experiments, brains were extracted one day postnatally. We quantified the number of EdU+ cells in the mPFC and their distribution by dividing the cortex into ten equal sized bins (Fig. 3B). Remarkably, PNS resulted in large scale reduction of cells born at E11.5 (Fig. 3C and D). Quantification of densities per bin showed that the decrease in EdU+ cell density was more pronounced mainly in deeper cortical layers (Fig. 3E). Interestingly, a compensatory effect was observed in later stages, characterized by an increase in EdU+ cells in PNS mice injected at E14.5 (Fig. 3F–H) and at E16.5 (Fig. 3I–K).

3.4. PNS differentially alters the density of MGE- and CGE-derived GABAergic neurons on P1

To determine if alterations in EdU+ cell density are unique to inhibitory neurons, we stained for inhibitory neurons markers as well (Fig. 4A). At P1, inhibitory neurons are still at the phase of maturation and migration, and can be identified by combinatorial expression of transcription factors (Kessaris et al., 2014) (Fig. 4B). Staining to Nr2f2 and Lhx6 enables differentiating between CGE-derived neurons (Nr2f2+, Lhx6-) and MGE-derived neurons, in specific, precursors of PV (Nr2f2-, Lhx6+) and of SST (Nr2f2+, Lhx6+) subpopulations.

We were able to show that PNS induced alteration in the ratio of CGE- and MGE-derived inhibitory neurons. Specifically, PNS increased the number of NR2F2+, Lhx6- (CGE-derived) neurons in the mPFC (Fig. 4C–E) while decreasing the number of LHX6+ (MGE-derived) neurons on postnatal day 1 (Fig. 4F–H). Interestingly, the ratio of SST+ neurons (a subtype of LHX6+ neurons also expressing NR2F2+) was not
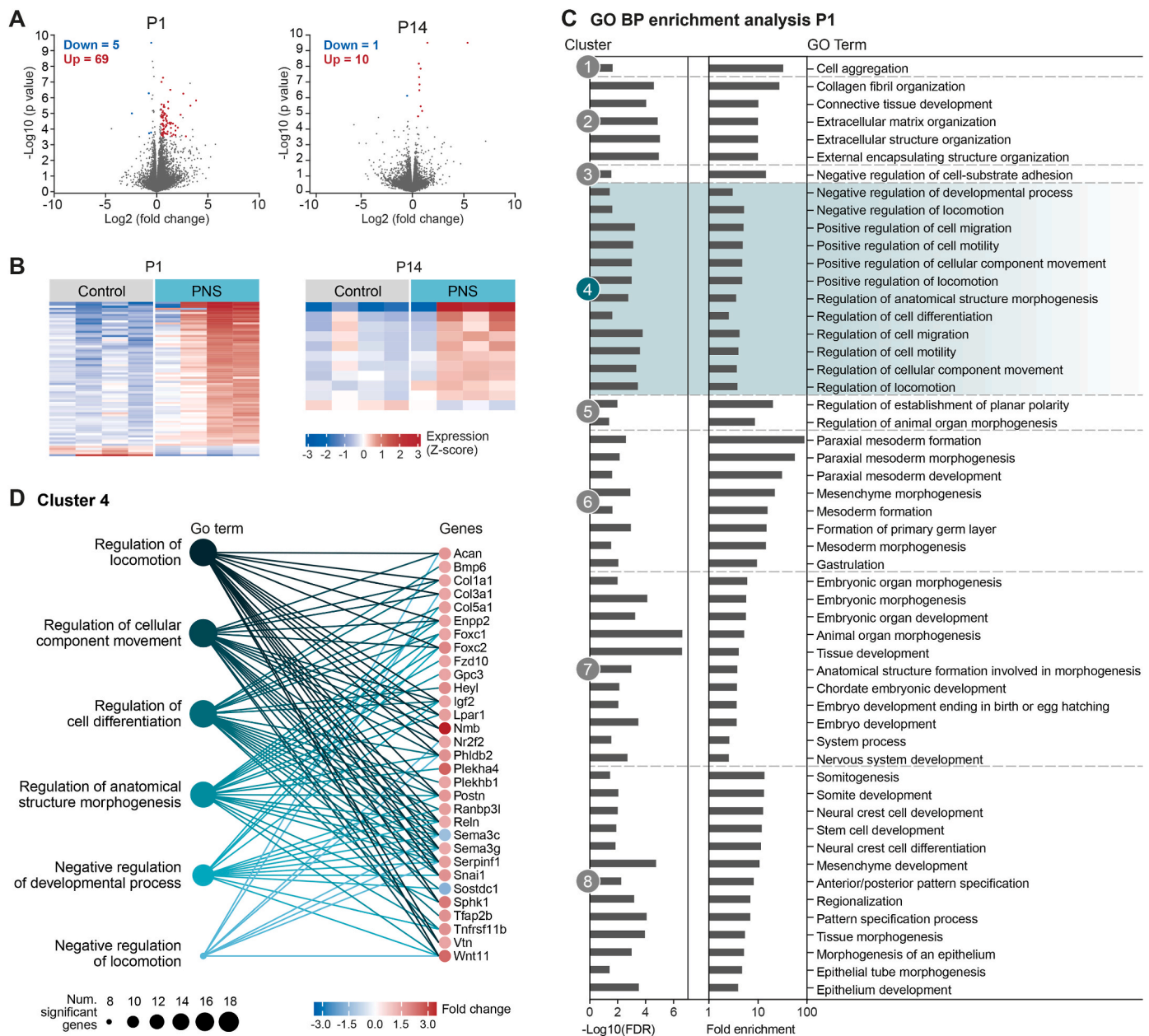
Fig. 2. PNS alters transcription of genes associated with cellular migration. (**A**) Volcano plots depicting differential expression of PNS vs. control at P1 (left) and P14 (Right). Each dot represents one gene. Differentially expressed genes were considered significant if adjusted p value ≤ 0.05, |fold change| ≥ 1.4 and the gene had at least one sample with 30 reads or more. Significantly DE genes are marked with red (upregulated) or blue (downregulated). (**B**) Heatmaps depicting expression level of significant DE genes in P1 (left) and P14 (right). Subjects are represented in columns, DE genes are represented in rows. (**C**) Gene ontology enrichment analysis at P1. Fifty-three significantly enriched GO terms are plotted with -log10(FDR) (left) and fold enrichment (right). Clusters based on DE gene similarity are separated by dashed lines and represented by numbers. (**D**) Network graph illustrating the relation between significant GO terms related to regulation of cell locomotion (e.g. cluster 4, left) to DE genes (right). If Go terms in the cluster were considered a parent and a child only the parent is presented. Circle size is correspondent to the number of significant genes related to that term. The 30 DE genes that relate to the term are depicted on the right, color represents fold change of PNS vs. control. GO terms are linked to the respective genes by lines.

affected by PNS, indicating that this effect was not uniform across all inhibitory neuron subtypes (Fig. 4I–K).

We further conducted an analysis comparing the proportion of cells labeled with EdU that also exhibited staining of inhibitory markers. The density of early born (e.g. E11.5) Lhx6+ neurons decreased due to PNS, whether they were Nr2f2 negative or positive, while the density of Nr2f2+/Lhx6- born at similar time were not affected (Fig. 4L–N). The density of inhibitory neuron populations born at E14.5 remained unaffected by PNS (Fig. 4O–Q). Finally, the density of Nr2f2+/Lhx6-neurons was increased by PNS specifically in late born cells (e.g. E16.5) with no

effect seen at that time point in Lhx6+ neurons (Fig. 4R–T). In conclusion, PNS induced alteration in the ratio of early born MGE- and late born CGE-derived inhibitory neurons at P1, suggesting a time specific vulnerability of distinct interneurons subtypes.

3.5. PNS induces a transient impairment of GABAergic interneurons subpopulations

Following the results observed at P1, we were also interested in examining if changes in cortical development obtained by PNS are
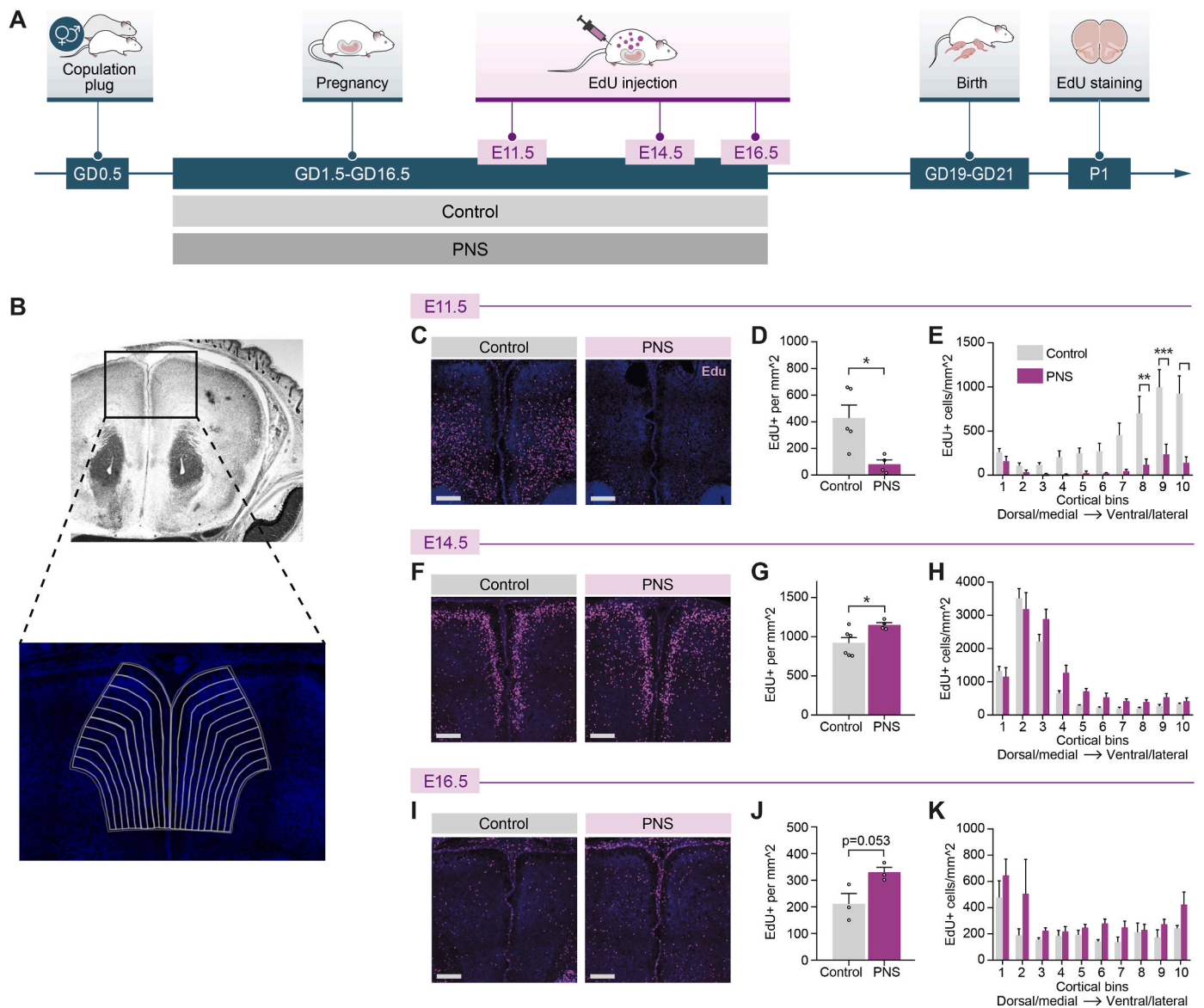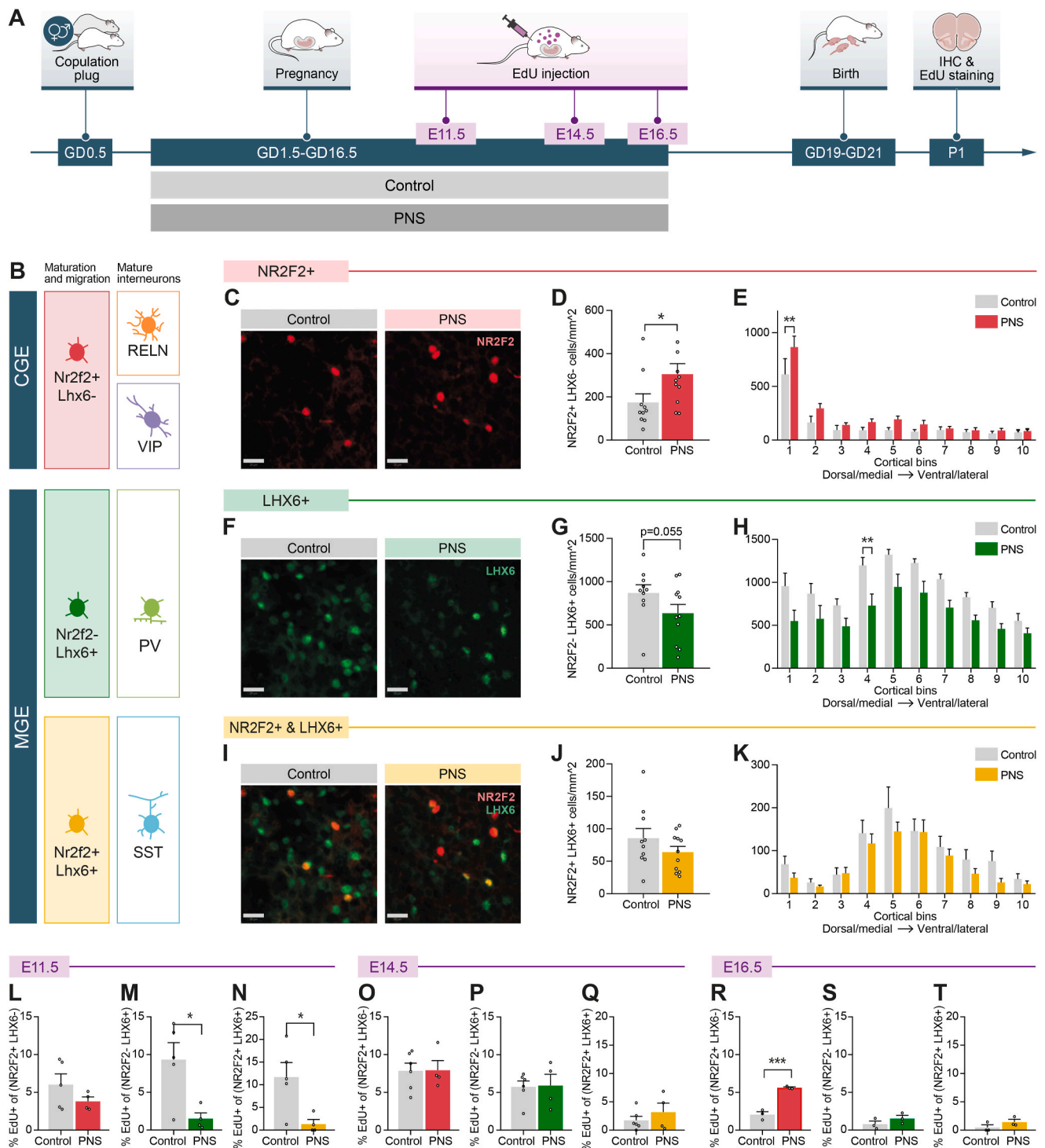
Fig. 3. PNS alters the density of cells born at various embryonic days in the mPFC at P1 (A) Experimental design. Dams undergo PNS protocol or are left undisturbed (contorl). Each damn is injected with EdU at one of three time-points: E11.5, E14.5 or E16.5. Brains of the offspring are taken for histology staining at P1. (B) Left and right mPFC are divided into 10 bins from the most dorsal/medial part to the ventral/lateral part. (C-E) Quantification of cells born at E11.5 as measured at P1. (C) Representative image of EdU Click-assay in control and PNS mice injected at E11.5. (D) Quantification of EdU+ cell density in the mPFC of mice injected at E11.5 (t(7) = 3.035 p = 0.019). (E) Quantification of EdU+ cell density by cortical bins of mice injected at E11.5 (Two-way ANOVA F(1,70) = 54.67 p < 0.0001). (F-H) Quantification of cells born at E14.5 as measured at P1. (F) Representative image of EdU Click-assay in control and PNS mice injected at E14.5. (G) Quantification of EdU+ cell density in the mPFC of mice injected at E14.5 (t(8) = 2.55 p = 0.034). (H) Quantification of EdU+ cell density by cortical bins of mice injected at E14.5 (F(1,80) = 9.177 p = 0.003). (I-K) Quantification of cells born at E16.5 as measured at P1. (I) Representative image of EdU Click-assay in control and PNS mice injected at E16.5. (J) Quantification of EdU+ cell density in the mPFC of mice injected at E16.5 (t(4) = 32.717 p = 0.053). (K) Quantification of EdU+ cell density by cortical bins of mice injected at E16.5 (F(1,40) = 10.38 p = 0.002). Scale is 200 μm. Bargraphs represent means, whiskers represent SEM. Asterix on graphs E,H,K represent Sidak's post-hoc test.

maintained until P15. We injected PNS and control mice with EdU at E11.5, E14.5, or E16.5, and brain extractions were performed at P15 (Fig. 5A). Quantification of EdU+ cell density in the mPFC revealed no significant differences in mice injected with EdU at E11.5 due to PNS (Fig. 5B and C). However, mice injected with EdU at E14.5 exhibited an increase in cell birth, consistent with the results observed at P1 (Fig. 5D and E). For cells born at E16.5, there was a trend toward increased density in PNS mice, similar to the pattern seen at P1, but this effect did not reach statistical significance (Fig. 5F and G), suggesting that the impact of PNS on inhibitory cell populations reduces by two weeks of age.

By two weeks of age, CGE- and MGE-derived interneurons express subtype specific genes (e.g. SST, PV, VIP, RELN) - indicating the differentiation to specific inhibitory neurons' subtypes. Therefore, we stained samples extracted at P15 for RELN, VIP, PV and SST, along with EdU click assay (Fig. 6A). Although a decrease in CGE derived neurons was observed at P1 in mice subjected to PNS, this difference was not observed when quantifying the two main CGE-derived subclasses at P15, either for RELN+ cells (Fig. 6B and C) nor VIP+ cells (Fig. 6E and F). When looking at cortical layers, the density of RELN+ was significantly decreased compared to control (Fig. 6D), but not the density of VIP+ neurons (Fig. 6G). Similarly, when quantifying the two main MGE-derived inhibitory subclasses, no changes were observed between PNS and control mice in the density and cortical distribution of PV+ cells

Fig. 4. **PNS differentially alters the density of GABAergic subtypes in the mPFC at P1 in a time-dependent manner.** (**A**) Experimental design. Dams undergo PNS protocol or are left undisturbed (control). Brains of the offspring are taken at P1 for histology staining of LHX6 and NR2F2, along with EdU click assay. (**B**) Markers for inhibitory neurons subtypes. LHX6 and NR2F2 transcription factors are expressed in premature neurons in the SVZ and are continuously expressed in maturing and migrating neurons in the cortical plate and into cortical layers. The main subtypes markers, including SST, PV, RELN and VIP are expressed in mature inhibitory neurons, the latest start to express at P14. (**C-E**) Quantification of NR2F2+/LHX6-cell density. (**C**) Representative image of NR2F2 IHC in control and PNS mice. (**D**) Quantification of cell density in the mPFC (t(19) = 2.052 p = 0.027). (**E**) Quantification of density by cortical bins (Two-way ANOVA F(1,170) = 11.9 p = 0.0007). (**F-H**) Quantification of NR2F2-/LHX6+ cell density. (**F**) Representative image of LHX6 IHC in control and PNS mice. (**G**) Quantification of cell density in the mPFC (t(19) = 1.677 p = 0.055). (**H**) Quantification of cell density by cortical bins (Two-way ANOVA F(1,170) = 4 7.07 p < 0.0001). (**I-K**) Quantification of NR2F2+/LHX6+ cell density. (**I**) Co-staining of NR2F2 and LhX6 IHC in control and PNS mice. (**J**) Quantification of cell density in the mPFC (t(19) = 1.263 p = 0.11). (**K**) Quantification of cell density by cortical bins (Two-way ANOVA F(1,170) = 6.174 p = 0.014). (**L-N**) Percentage of EdU+ cells of mice injected at E11.5 out of (**L**) NR2F2+/LHX6-, (**M**) NR2F2-/LHX6+ (t(7) = 2.987 p = 0.020) and (**N**) NR2F2+/LHX6+ (t(7) = 2.783 p = 0.027). (**O-Q**) Percent of EdU+ cells of mice injected at E14.5 out of (**O**) NR2F2+/LHX6-, (**P**) NR2F2-/LHX6+ and (**Q**) NR2F2+/LHX6+. (**R-T**) Percent of EdU+ cells of mice injected at E16.5 out of (**R**) NR2F2+/LHX6- (t(4) = 9.004 p = 0.0008), (**S**) NR2F2-/LHX6+ and (**T**) NR2F2+/LHX6+. Scale is 20 μm. Bargraphs represent means, whiskers represent SEM. Asterix on graphs E,H,K represent post-hoc corrected significance.
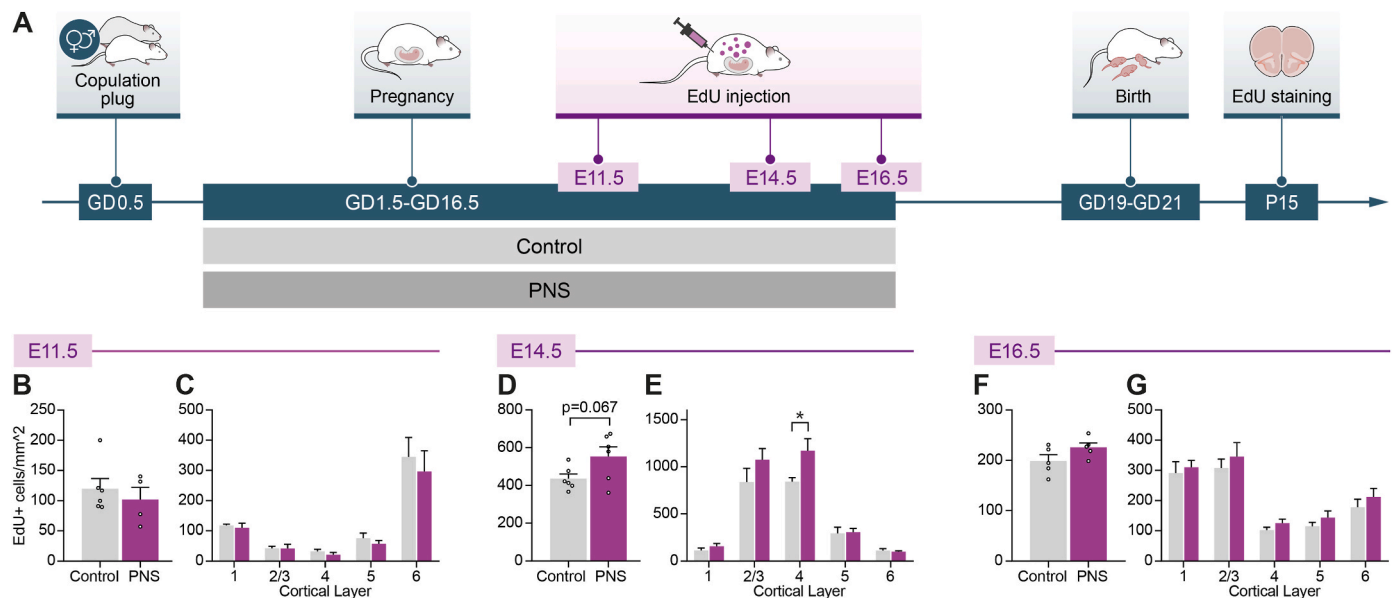
Fig. 5. The effect of PNS on cells born at various embryonic days in the mPFC is reduced by P15 (**A**) Experimental design. Dams undergo PNS protocol or are left undisturbed (control). Each damn is injected with EdU at one of three time-points: E11.5, E14.5 or E16.5. Brains of the offspring are taken at P15 for EdU staining. (**B-C**) Quantification of EdU+ cell density of mice injected at E11.5 in (**B**) the mPFC and (**C**) by cortical bins. (**D-E**) Quantification of EdU+ cell density of mice injected at E14.5 in (**D**) the mPFC and (**E**) by cortical bins ($F(1,50) = 6.058$ p $= 0.017$). (**F-G**) Quantification of EdU+ cell density of mice injected at E16.5 in (**F**) the mPFC and (**G**) by cortical bins ($F (1,40) = 2.763$, p $= 0.104$). Bargraphs represent means, whiskers represent SEM.

(Fig. 6H–J), nor in the density and cortical distribution of SST+ cells (Fig. 6K–M) This was ubiquitous to all cortical layers in the mPFC.

Lastly, we were interested in looking at the ratio of EdU+ cells specifically within inhibitory neurons subpopulation at P15. Analysis of co-staining resulted in an increase in the density of RELN+ neurons born specifically at E14.5 but not at other timepoints (Fig. 6N–P). A similar trend was also shown for VIP+ neurons (Fig. 6Q–S). Hence-the density of CGE-derived neurons is increased at P1 following PNS, whereas a similar trend is also observed at P15 in the differentiated sub-populations, specifically in those born at E14.5. No effect in newborn cells was observed at P14 for MGE derived inhibitory neurons, neither PV+ cells (Fig. 6T–V) nor SST+ cells (Fig. 6W–Y).

In summary, histological results from P1 and P15 indicate that the impact of PNS on cell birth is both subtype- and stage-specific, affecting cell density and distribution mainly at P1, with a diminished effect by P15.

4. Discussion

PNS has long been associated with adverse behavioral outcomes in the offspring, including increased risk to develop various disorders such as schizophrenia, MDD and anxiety disorders. Although the link between maternal mental state and offspring behavior is well established, the specific mechanisms through which maternal stress affects offspring brain development remain unclear. Rodent models provide an excellent framework for studying these effects, with chronic variable stress emerging as a widely used model for PNS. This model exposes pregnant rodents to unpredictable stressors over time and simulates the behavioral outcomes observed in humans exposed to PNS, including heightened anxiety- and depressive-like behaviors.

In this study, we employed a mouse model of chronic variable stress during pregnancy and showed an increase in anxiety- and depressive-like behavior in the adult male, but not female, offspring, as measured in the open field and forced swim tests. We identified significant transcriptional changes in the mPFC at P1 in genes related to cell migration and differentiation whereas many of these genes serve specifically in the development of inhibitory neurons (Kelsom and Lu, 2013; Vasistha and Khodosevich, 2021). These alterations were less pronounced at P14. We

further demonstrate an increase in CGE-derived neuron density at P1 in response to PNS, alongside decreased MGE-derived neuron density within the mPFC. Additionally, EdU labeling revealed time specific alterations in neuronal populations, with an underrepresentation of cells born at E11.5 and overrepresentation of cells born at later timepoints (E14.5, E16.5). By combining EdU labeling with inhibitory neuron markers, we demonstrated that the increase in the density of CGE-derived neuron was specifically from cells born at E16.5, while the decrease in MGE-derived neuronal density was predominantly from cells born at E11.5. These effects appear to be transient, as they were detected at P1 but to a lesser extent at P15.

Several studies previously demonstrated the effect of various stressors on inhibitory neuron populations within cortical layers. This includes immunogenic stress (Vasistha et al., 2019), cocaine and alcohol exposure as well as restraint stress. For example, immunogenic stress was shown to cause subtype and time specific effect on inhibitory neurons at several timepoints pre- and postnatally, affecting both MGE- and CGE-derived inhibitory neurons in the motor and sensory cortex (Vasistha et al., 2019). Prenatal restraint stress revealed a general decrease of telencephalic Gad67+ at E12.5, that was apparent up until P0 (Stevens et al., 2013). Additionally, restraint stress was shown to affect specifically the ratio of PV interneurons in the mPFC (Lussier and Stevens, 2016). Thus, inhibitory neurons display a vulnerability to alterations in the prenatal environment. In the current study we showed an effect that goes beyond PV neurons, illustrating a time- and subtype-specific sensitivity of inhibitory neurons to PNS.

MGE-derived neurons primarily mediate cortical inhibition, whereas CGE-derived neurons often facilitate disinhibition. Essentially, both alterations reported here, lead to a common outcome – a reduction in overall inhibition. These alterations at perinatal stages may lead to disruption of transient network formation that subsequently modulates maturation of cortical circuits (Bollmann et al., 2023; Duan et al., 2020). Even though fewer differences were observed at P15, changes in the density of inhibitory neuron subpopulations within the first two prenatal weeks can be sufficient in causing long lasting modifications in synaptic connectivity and neural circuit formation (Bollmann et al., 2023; Duan et al., 2020; Modol et al., 2020). These alterations may manifest later in development as disruptions in behavioral outcomes and susceptibility to
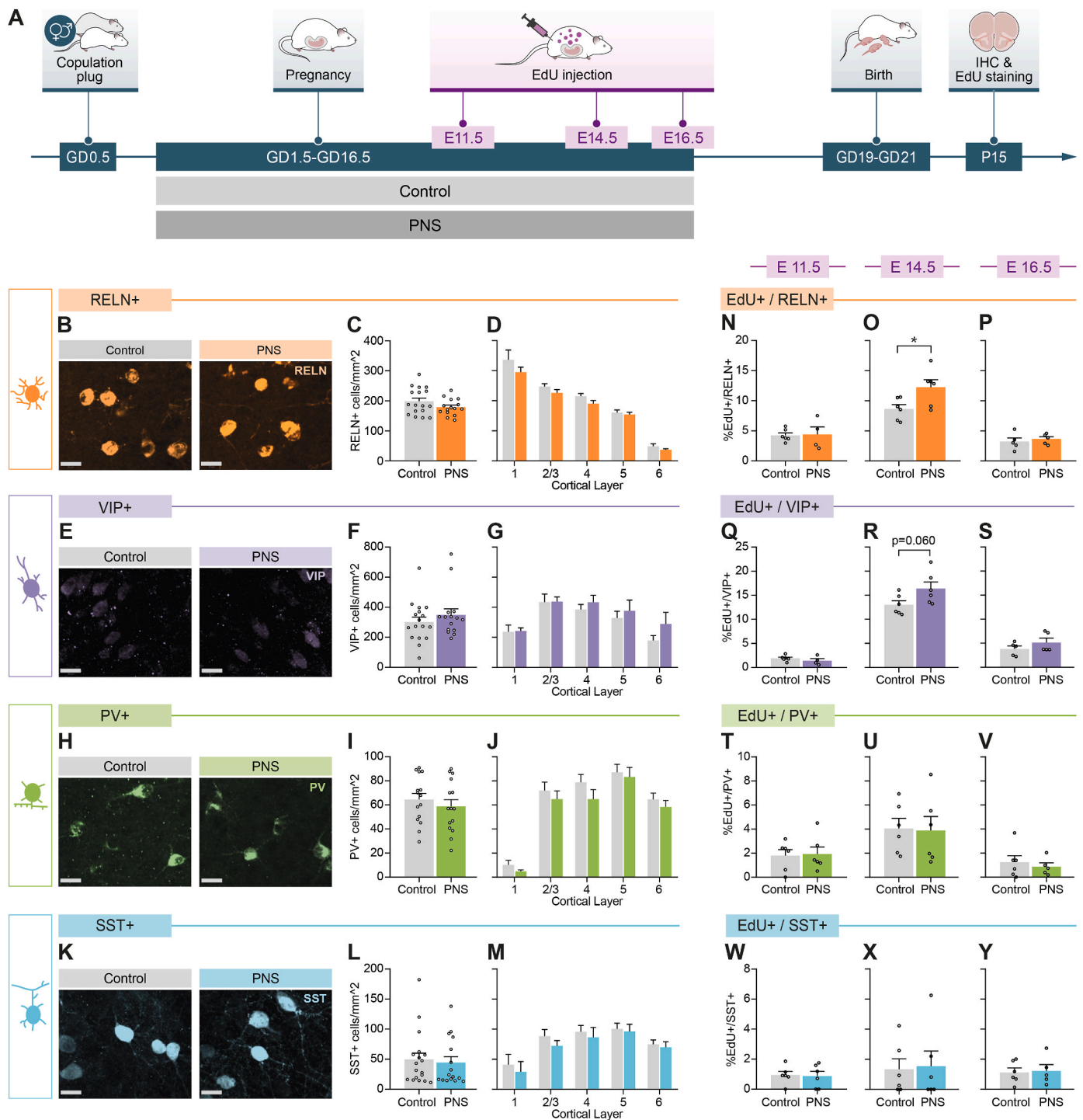
Fig. 6. The effect of PNS on interneuron development is transient and diminished by P15 (**A**) Experimental design. Dams undergo PNS protocol or are left undisturbed (control). Brains of the offspring are taken at P15 for immunostaining and EdU click assay (**B-D**) Quantification of RELN+ cells. (**B**) Representative image of control and PNS mPFC sections stained for RELN. (**C**) Quantification of RELN+ cell density in the mPFC, and (**D**) by cortical bins (Two-way ANOVA $F(1,150) = 5.269$ p = 0.0231). (**E-G**) Quantification of VIP+ cells. (**E**) Representative image of control and PNS mPFC sections stained for VIP. (**F**) Quantification of VIP+ cell density in the mPFC, and (**G**) by cortical bins. (**H-J**) Quantification of PV+ cells. (**H**) Representative image of control and PNS mPFC sections stained for PV. (**I**) Quantification of PV+ cell density in the mPFC, and (**J**) by cortical bins. (**K-M**) Quantification of SST+ cells. (**K**) Representative image of control and PNS mPFC sections stained for SST. (**L**) Quantification of SST+ cell density in the mPFC, and (**M**) by cortical bins. (**N-P**) Quantification of EdU+/RELN+ cells of mice injected at (**N**) E11.5, (**O**) E14.5 (t(10) = 2.507, p = 0.031) and (**P**) at E16.5. (**Q-S**) Quantification of EdU+/VIP+ cells of mice injected at (**Q**) E11.5, (**R**) E14.5 and (**S**) at E16.5. (**T-V**) Quantification of EdU+/PV+ cells of mice injected at (**T**) E11.5, (**U**) E14.5 and (**V**) at E16.5. (**W-Y**) Quantification of EdU+/SST+ cells of mice injected at (**W**) E11.5, (**X**) E14.5 and (**Y**) at E16.5. Scale is 20 μm. Bar-graphs represent means, whiskers represent SEM.

psychiatric disorders. Indeed, changes in connectivity in the mPFC is a phenotype strongly linked to schizophrenia and MDD (Hu et al., 2023; Liu et al., 2021), whereas PNS was linked to increased risk for both of these disorders (Brown et al., 1995; Franzek et al., 2008; Hoek et al., 1998; St Clair, 2005).

Following PNS, a lower density of cells born at E11.5 is evident in the mPFC by P1, mainly in ventral cortical layers. In contrast, an increased density of EdU+ cells is observed at P1 when EdU was introduced at E14.5 or E16.5. At P15 a difference in EdU+ density of mice injected at E14.5 was observed, yet other differences observed at P1 were diminished. The discrepancy between the densities of cells born at various embryonic stages and observed at P1 and P15 emphasizes the importance of developmental timing when interpreting long-term outcomes of PNS. Changes in cell density and distribution may be due to alterations in cell proliferation, cell migration and positioning, and cell death. Altered migration and positioning of inhibitory neurons could delay their integration into early cortical circuits. Given the critical role of interneurons in orchestrating spontaneous bursts and waves during development, even a transient shift in their distribution could disrupt circuit formation (Bollmann et al., 2023; Duan et al., 2020; Modol et al., 2020). Indeed, even single GABAergic "hub" cells can strongly modulate population dynamics in the developing cortex (Bollmann et al., 2023). In parallel, cell death is a major force in determining the final cell composition of cortical inhibitory circuits as it eliminates more than 40 % of initially generated inhibitory neurons (Southwell et al., 2012). Changes in the timing, extent, or selectivity of programmed cell death could therefore also contribute to the observed differences in interneuron density between P1 and P15. Further studies may elucidate the extent of each of these processes and their contribution to shaping network dynamics that underlie adult behavioral outcomes.

The effect of PNS on the birth of MGE-derived neurons is evident as early as E11.5 and can be observed at P1. Alternatively, PNS effect CGE-derived neurons that were born at a later time-point, notably E16.5, as observed at P1. This corresponds with the natural timing of interneuron generation, as MGE-derived neurons are born earlier than CGE-derived neurons. By P15, an increase is observed in RELN+ and VIP+ (both originate from the CGE) neurons born at E14.5, yet the remaining effects observed at P1 were diminished. This suggests that PNS exerts both immediate and transient effects on inhibitory neurons, highlighting the selective vulnerability of distinct interneuron populations at different developmental time points. Consistent with previous research, which demonstrated that PNS affects GABAergic neurons in a transient manner, the current findings reinforce the idea that certain interneuron subtypes are more susceptible to early-life stress during specific critical windows of development.

This temporal sensitivity extends beyond cellular effects, as the duration and timing of PNS also play a crucial role in shaping behavioral outcomes in adulthood (Lebow et al., 2024). Our model included stress throughout most of gestation and corroborates with previous studies that utilizes comparable duration of stress, thus emphasizing the significance of sustained PNS in shaping adult behavior. Previous work differs in the duration and severity of the stress applied to mothers, and consequently also in the phenotype observed in adult offspring mice, spanning from increase in stress related behaviors to changes in social and cognitive behaviors (Weinstock, 2008). For instance, PNS limited to a single trimester did not induce changes in anxiety like phenotype as measured by the OF test (Mueller and Bale, 2008), yet prolonged stress resulted in increased anxiety-like behavior, indicated by more time spent near walls (Lussier and Stevens, 2016). Similarly, stress exposure early or throughout gestation increased immobility in the FST, unlike exposure restricted to mid or late gestation periods (Mueller and Bale, 2008; Soares-Cunha et al., 2018).

Human and rodent studies have demonstrated a sexually dimorphic effect of PNS on offspring behavior (Glover and Hill, 2012; Weinstock, 2008). While several studies have reported non-sex-specific effects, other display sex-specific behavioral changes following PNS. Several factors mediate these differences, including the type of stressor, the timing during gestation and the duration. For instance, human studies conducted on the Dutch famine cohort have shown that PNS exposure during the first trimester was associated with increased rates of addiction in males but not females, while schizophrenia increased in females only (Franzek et al., 2008; Susser and Lin, 1992). Additionally, when the stress occurred during the second trimester, an increase in affective disorders was observed specifically in male (Brown et al., 1995). Animal models demonstrate a similar differential effect of PNS on males and females (Glover and Hill, 2012; Weinstock, 2008). These differences are thought to arise from the sexually dimorphic nature of brain development and hormonal regulation during gestation (Glover and Hill, 2012; McCormick et al., 1995; Welberg and Seckl, 2001). Using a model of chronic variable stress, we show that, under this specific protocol males are more prone to develop anxiety- and depressive-like behaviors. Therefore, we have focused our molecular and anatomical analysis on males. Nevertheless, exploring sex-specific responses to different types and durations of prenatal stress may provide a more comprehensive understanding of the long-term effects of PNS.

Finaly, our findings suggest that PNS transiently impairs interneuron development rather than causing permanent gross anatomical disruptions. While inhibitory neurons eventually reach their cortical destinations, transient changes in cell density of specific inhibitory subtypes may nonetheless affect network formation and synaptic integration, potentially underlying the behavioral deficits observed in adult offspring. This pattern of early anatomical recovery with lasting behavioral consequences emphasizes the role of critical periods and network formation in long-term behavioral outcomes. Better understanding these mechanisms may ultimately contribute to the identification of sensitive developmental windows and targets for early intervention.

CRediT authorship contribution statement

Keren Shoshani-Haye: Writing – review & editing, Writing – original draft, Visualization, Methodology, Investigation, Formal analysis, Conceptualization. **Gilgi Friedlander:** Visualization, Software, Formal analysis. **Ofra Golani:** Software, Methodology, Formal analysis. **Suellen Almeida-Correa:** Methodology, Investigation. **Yair Shemesh:** Writing – review & editing, Methodology, Investigation, Conceptualization. **Alon Chen:** Writing – review & editing, Supervision, Project administration, Funding acquisition, Conceptualization.

Declaration of competing interest

The authors declare that they have no known competing financial interests or personal relationships that could have appeared to influence the work reported in this paper.

Acknowledgments

advice and insightful discussions. Optical imaging data was acquired at the de Picciotto Cancer Cell Observatory In memory of Wolfgang and Ruth Lesser of the Moross Integrated Cancer Center at Weizmann Institute of Science. We thank the members of the Chen Lab for helpful discussion and support.

Appendix A. Supplementary data

Supplementary data to this article can be found online at https://doi.org/10.1016/j.ynstr.2025.100749.

Data availability

RNA Sequencing data are accessible in the Gene Expression Omnibus (GEO) repository under the accession number GEO: GSE296365.

References

Almond, D., Currie, J., 2011. Killing me softly: the fetal origins hypothesis. J. Econ. Perspect. 25, 153. https://doi.org/10.1257/JEP.25.3.153.

Anders, S., Pyl, P.T., Huber, W., 2015. HTSeq-A Python framework to work with high-throughput sequencing data. Bioinformatics 31, 166–169. https://doi.org/10.1093/BIOINFORMATICS/BTU638.

Ashburner, M., Ball, C.A., Blake, J.A., Botstein, D., Butler, H., Cherry, J.M., Davis, A.P., Dolinski, K., Dwight, S.S., Eppig, J.T., Harris, M.A., Hill, D.P., Issel-Tarver, L., Kasarskis, A., Lewis, S., Matese, J.C., Richardson, J.E., Ringwald, M., Rubin, G.M., Sherlock, G., 2000. Gene ontology: tool for the unification of biology. The gene Ontology Consortium. Nat. Genet. 25, 25–29. https://doi.org/10.1038/75556.

Bai, M., Yu, H., Chen, C., Xu, X., He, Y., Wang, Y., Tian, Y., Wu, Z., Lan, T., Li, Y., Chen, X., Chen, Z., Zhao, L., Fang, L., Yang, D., Cheng, K., Xie, P., 2022. Pigment epithelium-derived factor may induce antidepressant phenotypes in mice by the prefrontal cortex. Neurosci. Lett. 771, 136423. https://doi.org/10.1016/J.NEULET.2021.136423.

Bankhead, P., Loughrey, M.B., Fernández, J.A., Dombrowski, Y., McArt, D.G., Dunne, P.D., McQuaid, S., Gray, R.T., Murray, L.J., Coleman, H.G., James, J.A., Salto-Tellez, M., Hamilton, P.W., 2017. QuPath: open source software for digital pathology image analysis. Sci. Rep. 71 (7), 1–7. https://doi.org/10.1038/s41598-017-17204-5.

Birnie, M.T., Baram, T.Z., 2025. The evolving neurobiology of early-life stress. Neuron 113, 1474–1490. https://doi.org/10.1016/J.NEURON.2025.02.016.

Birnie, M.T., Baram, T.Z., 2022. Principles of emotional brain circuit maturation. Science 376, 1055–1056. https://doi.org/10.1126/SCIENCE.ABN4016.

Boersma, G.J., Tamashiro, K.L., 2015. Individual differences in the effects of prenatal stress exposure in rodents. Neurobiol. Stress 1, 100–108. https://doi.org/10.1016/j.ynstr.2014.10.006.

Bollmann, Y., Modol, L., Tressard, T., Vorobyev, A., Dard, R., Brustlein, S., Sims, R., Bendifallah, I., Leprince, E., de Sars, V., Ronzitti, E., Baude, A., Adesnik, H., Picardo, M.A., Platel, J.C., Emiliani, V., Angulo-Garcia, D., Cossart, R., 2023. Prominent in vivo influence of single interneurons in the developing barrel cortex. Nat. Neurosci. 26, 1555–1565. https://doi.org/10.1038/S41593-023-01405-5.

Brown, A.S., Susser, E.S., Lin, S.P., Neugebauer, R., Gorman, J.M., 1995. Increased risk of affective disorders in males after second trimester prenatal exposure to the Dutch hunger winter of 1944-45. Br. J. Psychiatry 166, 601–606. https://doi.org/10.1192/bjp.166.5.601.

Buss, C., Davis, E.P., Shahbaba, B., Pruessner, J.C., Head, K., Sandman, C.A., 2012. Maternal cortisol over the course of pregnancy and subsequent child amygdala and hippocampus volumes and affective problems. Proc. Natl. Acad. Sci. U. S. A. 109, E1312. https://doi.org/10.1073/PNAS.1201295109.

Carbon, S., Douglass, E., Good, B.M., Unni, D.R., Harris, N.L., Mungall, C.J., Basu, S., Chisholm, R.L., Dodson, R.J., Hartline, E., Fey, P., Thomas, P.D., Albou, L.P., Ebert, D., Kesling, M.J., Mi, H., Muruganujan, A., Huang, X., Mushayahama, T., LaBonte, S.A., Siegele, D.A., Antonazzo, G., Attrill, H., Brown, N.H., Garapati, P., Marygold, S.J., Trovisco, V., dos Santos, G., Falls, K., Tabone, C., Zhou, P., Goodman, J.L., Strelets, V.B., Thurmond, J., Garmiri, P., Ishtiaq, R., Rodríguez-López, M., Acencio, M.L., Kuiper, M., Lægreid, A., Logie, C., Lovering, R.C., Kramarz, B., Saverimuttu, S.C.C., Pinheiro, S.M., Gunn, H., Su, R., Thurlow, K.E., Chibucos, M., Giglio, M., Nadendla, S., Munro, J., Jackson, R., Duesbury, M.J., Del-Toro, N., Meldal, B.H.M., Paneerselvam, K., Perfetto, L., Porras, P., Orchard, S., Shrivastava, A., Chang, H.Y., Finn, R.D., Mitchell, A.L., Rawlings, N.D., Richardson, L., Sangrador-Vegas, A., Blake, J.A., Christie, K.R., Dolan, M.E., Drabkin, H.J., Hill, D.P., Ni, L., Sitnikov, D.M., Harris, M.A., Oliver, S.G., Rutherford, K., Wood, V., Hayles, J., Bähler, J., Bolton, E.R., de Pons, J.L., Dwinell, M.R., Hayman, G.T., Kaldunski, M.L., Kwitek, A.E., Laulederkind, S.J.F., Plasterer, C., Tutaj, M.A., Vedi, M., Wang, S.J., D'Eustachio, P., Matthews, L., Balhoff, J.P., Aleksander, S.A., Alexander, J.M., Cherry, J.M., Engel, S.R., Gondwe, F., Karra, K., Miyasato, S.R., Nash, R.S., Simison, M., Skrzypek, M.S., Weng, S., Wong, E.D., Feuermann, M., Gaudet, P., Morgat, A., Bakker, E., Berardini, T.Z., Reiser, L., Subramaniam, S., Huala, E., Arighi, C.N., Auchincloss, A., Axelsen, K., Argoud-Puy, G., Bateman, A., Blatter, M.C., Boutet, E., Bowler, E., Breuza, L., Bridge, A., Britto, R., Bye-A-Jee, H., Casas, C.C., Coudert, E., Denny, P., Es-Treicher, A., Famiglietti, M.L., Georghiou, G., Gos, A.N., Gruaz-Gumowski, N., Hatton-Ellis, E., Hulo, C., Ignatchenko, A., Jungo, F., Laiho, K., Le Mercier, P.,

Lieberherr, D., Lock, A., Lussi, Y., MacDougall, A., Ma-Grane, M., Martin, M.J., Masson, P., Natale, D.A., Hyka-Nouspikel, N., Orchard, S., Pedruzzi, I., Pourcel, L., Poux, S., Pundir, S., Rivoire, C., Speretta, E., Sundaram, S., Tyagi, N., Warner, K., Zaru, R., Wu, C.H., Diehl, A.D., Chan, J.N., Grove, C., Lee, R.Y.N., Muller, H.M., Gao, S., Wright, A., Stein, L., Howe, D.G., Toro, S., Westerfield, M., Jaiswal, P., Cooper, L., Elser, J., 2021. The Gene Ontology resource: enriching a GOld mine. Nucleic Acids Res. 49, D325–D334. https://doi.org/10.1093/NAR/GKAA1113.

Chiaruttini, N., Burri, O., Haub, P., Guiet, R., Sordet-Dessimoz, J., Seitz, A., 2022. An open-source whole slide image registration workflow at cellular precision using Fiji, QuPath and elastix. Front. Comput. Sci. 3, 780026. https://doi.org/10.3389/FCOMP.2021.780026.

Davis, E.P., Stout, S.A., Molet, J., Vegetabile, B., Glynn, L.M., Sandman, C.A., Heins, K., Stern, H., Baram, T.Z., 2017. Exposure to unpredictable maternal sensory signals influences cognitive development across species. Proc. Natl. Acad. Sci. U. S. A. 114, 10390–10395. https://doi.org/10.1073/PNAS.1703444114.

Dobin, A., Davis, C.A., Schlesinger, F., Drenkow, J., Zaleski, C., Jha, S., Batut, P., Chaisson, M., Gingeras, T.R., 2013. STAR: ultrafast universal RNA-seq aligner. Bioinformatics 29, 15–21. https://doi.org/10.1093/BIOINFORMATICS/BTS635.

Duan, Z.R.S., Che, A., Chu, P., Modol, L., Bollmann, Y., Babij, R., Fetcho, R.N., Otsuka, T., Fuccillo, M.V., Liston, C., Pisapia, D.J., Cossart, R., De Marco García, N.V., 2020. GABAergic restriction of network dynamics regulates Interneuron survival in the developing cortex. Neuron 105, 75–92.e5. https://doi.org/10.1016/j.neuron.2019.10.008.

Edgar, R., Domrachev, M., Lash, A.E., 2002. Gene Expression Omnibus: NCBI gene expression and hybridization array data repository. Nucleic Acids Res. 30, 207–210. https://doi.org/10.1093/NAR/30.1.207.

Enayati, M., Mosaferi, B., Homberg, J.R., Diniz, D.M., Salari, A.A., 2020. Prenatal maternal stress alters depression-related symptoms in a strain - and sex-dependent manner in rodent offspring. Life Sci. 251. https://doi.org/10.1016/j.lfs.2020.117597.

Estanislau, C., Morato, S., 2005. Prenatal stress produces more behavioral alterations than maternal separation in the elevated plus-maze and in the elevated T-maze. Behav. Brain Res. 163, 70–77. https://doi.org/10.1016/j.bbr.2005.04.003.

Franzek, E.J., Sprangers, N., Janssens, A.C.J.W., Van Duijn, C.M., Van De Wetering, B.J.M., 2008. Prenatal exposure to the 1944-45 Dutch 'hunger winter' and addiction later in life. Addiction 103, 433–438. https://doi.org/10.1111/j.1360-0443.2007.02084.x.

Fraser, A., Macdonald-wallis, C., Tilling, K., Boyd, A., Golding, J., Davey smith, G., Henderson, J., Macleod, J., Molloy, L., Ness, A., Ring, S., Nelson, S.M., Lawlor, D.A., 2012. Cohort profile: the Avon Longitudinal Study of Parents and Children: ALSPAC mothers cohort. Int. J. Epidemiol. 42, 97. https://doi.org/10.1093/IJE/DYS066.

Glover, V., Hill, J., 2012. Sex differences in the programming effects of prenatal stress on psychopathology and stress responses: an evolutionary perspective. Physiol. Behav. 106, 736–740. https://doi.org/10.1016/J.PHYSBEH.2012.02.011.

Greenman, R., Gorelik, A., Sapir, T., Baumgart, J., Zamor, V., Segal-Salto, M., Levin-Zaidman, S., Aidinis, V., Aoki, J., Nitsch, R., Vogt, J., Reiner, O., 2015. Non-cell autonomous and non-catalytic activities of ATX in the developing brain. Front. Neurosci. 9. https://doi.org/10.3389/FNINS.2015.00053.

Gu, Z., 2022. Complex heatmap visualization. iMeta 1, e43. https://doi.org/10.1002/IMT2.43.

Gu, Z., Eils, R., Schlesner, M., 2016. Complex heatmaps reveal patterns and correlations in multidimensional genomic data. Bioinformatics 32, 2847–2849. https://doi.org/10.1093/BIOINFORMATICS/BTW313.

Hoek, H.W., Brown, A.S., Susser, E., 1998. The Dutch Famine and schizophrenia spectrum disorders. Soc. Psychiatry Psychiatr. Epidemiol. 33, 373–379. https://doi.org/10.1007/s001270050068.

Hu, Y.T., Tan, Z.L., Hirjak, D., Northoff, G., 2023. Brain-wide changes in excitation-inhibition balance of major depressive disorder: a systematic review of topographic patterns of GABA- and glutamatergic alterations. Mol. Psychiatr. 288 (28), 3257–3266. https://doi.org/10.1038/s41380-023-02193-x.

Jafari, Z., Mehla, J., Kolb, B.E., Mohajerani, M.H., 2017. Prenatal noise stress impairs HPA axis and cognitive performance in mice. Sci. Rep. 71 (7), 1–13. https://doi.org/10.1038/s41598-017-09799-6.

Kelsom, C., Lu, W., 2013. Development and specification of GABAergic cortical interneurons. Cell Biosci. 31 (3), 1–19. https://doi.org/10.1186/2045-3701-3-19.

Kessaris, N., Magno, L., Rubin, A.N., Oliveira, M.G., 2014. Genetic programs controlling cortical interneuron fate. Curr. Opin. Neurobiol. 26, 79–87. https://doi.org/10.1016/J.CONB.2013.12.012.

Kolominsky, Y., Igumnov, S., Drozdovitch, V., 1999. The psychological development of children from Belarus exposed in the prenatal period to radiation from the Chernobyl Atomic power plant. J. Child Psychol. Psychiatry 40, 299–305. https://doi.org/10.1017/S0021963098003369.

Laclef, C., Métin, C., 2018. Conserved rules in embryonic development of cortical interneurons. Semin. Cell Dev. Biol. 76, 86–100. https://doi.org/10.1016/J.SEMCDB.2017.09.017.

Lebow, M., Kuperman, Y., Chen, A., 2024. Prenatal-induced psychopathologies: all roads lead to microglia. Stress Immunol. Inflamm. Handb. Stress Ser. 5 (5), 199–214. https://doi.org/10.1016/B978-0-12-817558-3.00016-0.

Lim, L., Mi, D., Llorca, A., Marín, O., 2018. Development and functional diversification of cortical interneurons. Neuron 100, 294. https://doi.org/10.1016/J.NEURON.2018.10.009.

Liu, Y., Ouyang, P., Zheng, Y., Mi, L., Zhao, J., Ning, Y., Guo, W., 2021. A selective review of the excitatory-inhibitory imbalance in schizophrenia: underlying biology, genetics, microcircuits, and symptoms. Front. Cell Dev. Biol. 9. https://doi.org/10.3389/FCELL.2021.664535.

Llorca, A., Deogracias, R., 2022. Origin, development, and synaptogenesis of cortical interneurons. Front. Neurosci. 16. https://doi.org/10.3389/FNINS.2022.929469.

Love, M.I., Huber, W., Anders, S., 2014. Moderated estimation of fold change and dispersion for RNA-seq data with DESeq2. Genome Biol. 15, 1–21. https://doi.org/10.1186/S13059-014-0550-8.

Lussier, S.J., Stevens, H.E., 2016. Delays in GABAergic interneuron development and behavioral inhibition after prenatal stress. Dev. Neurobiol. 76, 1078–1091. https://doi.org/10.1002/DNEU.22376.

Markham, J.A., Koenig, J.I., 2010. Prenatal stress: role in psychotic and depressive diseases. Psychopharmacol. Ser. 2141 (214), 89–106. https://doi.org/10.1007/S00213-010-2035-0.

Martin, M., 2011. Cutadapt removes adapter sequences from high-throughput sequencing reads. EMBnet. J. 17, 10–12. https://doi.org/10.14806/EJ.17.1.200.

McCarthy, D.M., Zhang, X., Darnell, S.B., Sangrey, G.R., Yanagawa, Y., Sadri-Vakili, G., Bhide, P.G., 2011. Cocaine alters BDNF expression and neuronal migration in the embryonic mouse forebrain. J. Neurosci. 31, 13400–13411. https://doi.org/10.1523/JNEUROSCI.2944-11.2011.

McCormick, C.M., Smythe, J.W., Sharma, S., Meaney, M.J., 1995. Sex-specific effects of prenatal stress on hypothalamic-pituitary-adrenal responses to stress and brain glucocorticoid receptor density in adult rats. Dev. Brain Res. 84, 55–61. https://doi.org/10.1016/0165-3806(94)00153-Q.

Miyoshi, G., Fishell, G., 2011. GABAergic interneuron lineages selectively sort into specific cortical layers during early postnatal development. Cereb. Cortex 21, 845–852. https://doi.org/10.1093/CERCOR/BHQ155.

Miyoshi, G., Hjerling-Leffler, J., Karayannis, T., Sousa, V.H., Butt, S.J.B., Battiste, J., Johnson, J.E., Machold, R.P., Fishell, G., 2010. Genetic fate mapping reveals that the caudal ganglionic eminence produces a large and diverse population of superficial cortical interneurons. J. Neurosci. 30, 1582. https://doi.org/10.1523/JNEUROSCI.4515-09.2010.

Modol, L., Bollmann, Y., Tressard, T., Baude, A., Che, A., Duan, Z.R.S., Babij, R., De Marco García, N.V., Cossart, R., 2020. Assemblies of perisomatic GABAergic neurons in the developing barrel cortex. Neuron 105, 93–105.e4. https://doi.org/10.1016/j.neuron.2019.10.007.

Mölder, F., Jablonski, K.P., Letcher, B., Hall, M.B., Tomkins-Tinch, C.H., Sochat, V., Forster, J., Lee, S., Twardziok, S.O., Kanitz, A., Wilm, A., Holtgrewe, M., Rahmann, S., Nahnsen, S., Köster, J., 2021. Sustainable data analysis with snakemake. F1000Research 10, 33. https://doi.org/10.12688/f1000research.29032.2.

Morley-Fletcher, S., Darnaudéry, M., Mocaer, E., Froger, N., Lanfumey, L., Laviola, G., Casolini, P., Zuena, A.R., Marzano, L., Hamon, M., Maccari, S., 2004. Chronic treatment with imipramine reverses immobility behaviour, hippocampal corticosteroid receptors and cortical 5-HT1A receptor mRNA in prenatally stressed rats. Neuropharmacology 47, 841–847. https://doi.org/10.1016/j.neuropharm.2004.06.011.

Mueller, B.R., Bale, T.L., 2008. Sex-specific programming of offspring emotionality after stress early in pregnancy. J. Neurosci. 28, 9055–9065. https://doi.org/10.1523/JNEUROSCI.1424-08.2008.

Pardo, M., Cheng, Y., Sitbon, Y.H., Lowell, J.A., Grieco, S.F., Worthen, R.J., Desse, S., Barreda-Diaz, A., 2019. Insulin growth factor 2 (IGF2) as an emergent target in psychiatric and neurological disorders. Review. Neurosci. Res. 149, 1–13. https://doi.org/10.1016/J.NEURES.2018.10.012.

Paxinos, G., Halliday, G., Watson, C., Kassem, M.S., 2020. Atlas of the developing mouse brain. Atlas Dev. Mouse Brain 1–384.

Schindelin, J., Arganda-Carreras, I., Frise, E., Kaynig, V., Longair, M., Pietzsch, T., Preibisch, S., Rueden, C., Saalfeld, S., Schmid, B., Tinevez, J.Y., White, D.J., Hartenstein, V., Eliceiri, K., Tomancak, P., Cardona, A., 2012. Fiji: an open-source platform for biological-image analysis. Nat. Methods 97 (9), 676–682. https://doi.org/10.1038/nmeth.2019.

Schroeder, M., Jakovcevski, M., Polacheck, T., Drori, Y., Ben-Dor, S., Röh, S., Chen, A., 2018a. Sex dependent impact of gestational stress on predisposition to eating disorders and metabolic disease. Mol. Metab. 17, 1–16. https://doi.org/10.1016/J.MOLMET.2018.08.005.

Schroeder, M., Jakovcevski, M., Polacheck, T., Drori, Y., Luoni, A., Röh, S., Zaugg, J., Ben-Dor, S., Albrecht, C., Chen, A., 2018b. Placental miR-340 mediates vulnerability to activity based anorexia in mice. Nat. Commun. 9. https://doi.org/10.1038/s41467-018-03836-2.

Seckl, J.R., Meaney, M.J., 2004. Glucocorticoid programming. Ann. N. Y. Acad. Sci. 1032, 63–84. https://doi.org/10.1196/ANNALS.1314.006.

Seibenhener, M.L., Wooten, M.C., 2015. Use of the open field maze to measure locomotor and anxiety-like behavior in mice. J. Vis. Exp. 6, e52434. https://doi.org/10.3791/52434.

Soares-Cunha, C., Coimbra, B., Borges, S., Domingues, A.V., Silva, D., Sousa, N., Rodrigues, A.J., 2018. Mild prenatal stress causes emotional and brain structural modifications in rats of both sexes. Front. Behav. Neurosci. 12, 373924. https://doi.org/10.3389/FNBEH.2018.00129.

Southwell, D.G., Paredes, M.F., Galvao, R.P., Jones, D.L., Froemke, R.C., Sebe, J.Y., Alfaro-Cervello, C., Tang, Y., Garcia-Verdugo, J.M., Rubenstein, J.L., Baraban, S.C., Alvarez-Buylla, A., 2012. Intrinsically determined cell death of developing cortical interneurons. Nat 2012, 109–113. https://doi.org/10.1038/nature11523, 4917422 491.

St Clair, D., 2005. Rates of adult schizophrenia following prenatal exposure to the Chinese famine of 1959-1961. JAMA 294, 557. https://doi.org/10.1001/jama.294.5.557.

Stevens, H.E., Su, T., Yanagawa, Y., Vaccarino, F.M., 2013. Prenatal stress delays inhibitory neuron progenitor migration in the developing neocortex. Psychoneuroendocrinology 38, 509–521. https://doi.org/10.1016/J.PSYNEUEN.2012.07.011.

Susser, E.S., Lin, S.P., 1992. Schizophrenia after prenatal exposure to the Dutch hunger Winter of 1944-1945. Arch. Gen. Psychiatry 49, 983–988. https://doi.org/10.1001/ARCHPSYC.1992.01820120071010.

Van den Hove, D.L.A., Kenis, G., Brass, A., Opstelten, R., Rutten, B.P.F., Bruschettini, M., Blanco, C.E., Lesch, K.P., Steinbusch, H.W.M., Prickaerts, J., 2013. Vulnerability versus resilience to prenatal stress in male and female rats; implications from gene expression profiles in the hippocampus and frontal cortex. Eur. Neuropsychopharmacol. 23, 1226–1246. https://doi.org/10.1016/j.euroneuro.2012.09.011.

Vasistha, N.A., Khodosevich, K., 2021. The impact of (ab)normal maternal environment on cortical development. Prog. Neurobiol. 202, 102054. https://doi.org/10.1016/J.PNEUROBIO.2021.102054.

Vasistha, N.A., Pardo-Navarro, M., Gasthaus, J., Weijers, D., Müller, M.K., García-González, D., Malwade, S., Korshunova, I., Pfisterer, U., von Engelhardt, J., Hougaard, K.S., Khodosevich, K., 2019. Maternal inflammation has a profound effect on cortical interneuron development in a stage and subtype-specific manner. Mol. Psychiatr. 2510 (25), 2313–2329. https://doi.org/10.1038/s41380-019-0539-5.

Weigert, M., Schmidt, U., 2022. Nuclei instance segmentation and classification in histopathology images with StarDist. ISBIC 2022 - int. Symp. Biomed. Imaging challenges. SAVE Proc. https://doi.org/10.1109/ISBIC56247.2022.9854534.

Weinstock, M., 2017. Prenatal stressors in rodents: effects on behavior. Neurobiol. Stress 6, 3–13. https://doi.org/10.1016/j.ynstr.2016.08.004.

Weinstock, M., 2008. The long-term behavioural consequences of prenatal stress. Neurosci. Biobehav. Rev. 32, 1073–1086. https://doi.org/10.1016/J.NEUBIOREV.2008.03.002.

Welberg, L.A.M., Seckl, J.R., 2001. Prenatal stress, glucocorticoids and the programming of the brain. J. Neuroendocrinol. 13, 113–128. https://doi.org/10.1111/J.1365-2826.2001.00601.X.

Zuena, A.R., Mairesse, J., Casolini, P., Cinque, C., Alemà, G.S., Morley-Fletcher, S., Chiodi, V., Spagnoli, L.G., Gradini, R., Catalani, A., Nicoletti, F., Maccari, S., 2008. Prenatal restraint stress generates two distinct behavioral and neurochemical profiles in Male and female rats. PLoS One 3, e2170. https://doi.org/10.1371/journal.pone.0002170.